Play Fairway Analysis of Steptoe Valley, Nevada: Integrating Geology, Geochemistry, Geophysics, and Heat Flow Modeling in the Search for Blind Resources

Nicholas H. Hinz[1,2], James E. Faulds[2], Mark F. Coolbaugh[2], Christian Hardwick[3], Mark Gwynn[3,4], John Queen[4], Bridget Ayling[2]

[1]Geologica Geothermal Group, Inc.

[2]Great Basin Center for Geothermal Energy, Nevada Bureau of Mines and Geology, University of Nevada, Reno

[3]Utah Geological Survey

[4]Utah Division of Oil, Gas and Mining

[5]Hi-Q Geophysical, Inc.

Keywords

Play Fairway Analysis, Sedimentary Basin, Structural Controls, Carbonate Aquifer, Blind Geothermal System

ABSTRACT

Steptoe Valley was one of five areas selected for detailed study from an initial 96,000 km^2 Nevada play fairway study completed in 2015. The purposes of conducting the detailed field studies were to increase the level of data resolution and increase the quality or confidence in the inputs in this play fairway analysis. The Steptoe Valley study area boundaries were selected 1) to include several highly favorable areas identified in the initial regional study, 2) where substantial subsurface data were available, including existing borehole data and 2D seismic reflection profiles, and 3) to include the deep part of northern Steptoe Valley that has been the focus of sedimentary basin geothermal resource studies. New detailed mapping of the range-front fault system provided better resolution with conspicuous steps in the main fault trace ranging up to 500 m. Nearly 300 new gravity stations were collected and merged with existing data to support multiple types of models. Nearly 200 km of seismic reflection data were interpreted with control provided by mapping, well data, and gravity modeling. 3D geologic modeling was employed to integrate the geologic map data, well data, and 2D reflection profiles to map the intrabasinal fault architecture, and to support a study-area-wide conductive heat flow model. Twelve favorable structural settings were defined from the new 2D and 3D geologic map. Two of these are associated with known geothermal areas (Monte Neva and Cherry Creek Hot Springs), the rest may host undiscovered blind resources. GeoT equilibrium modeling of fluids from Cherry Creek and Monte Neva Hot Springs both indicate that power capable (>130 °C) reservoirs are possible.

1. Introduction

Steptoe Valley was one of five areas selected for detailed study from the initial 96,000 km^2 Nevada Play Fairway study area (Figure 1; Faulds et al., 2015a). The purpose of the regional study was to develop a method of estimating probability of an area hosting a power capable (≥130 °C) geothermal resource, including blind or hidden systems. The four other sites selected for detailed study include Granite Springs Valley (Faulds et al., 2019), Crescent Valley (McConville et al., 2017; McConville, 2018), southern Gabbs Valley (Craig et al., 2017; Craig, 2018), and Sou Hills (Faulds et al., this volume; Figure 1). These five areas were selected from among many favorable areas identified across the initial study area to include broad geographical distribution that incorporated variations in tectonic setting (transtensional vs. purely extensional), strain rates, composition of basement rocks, and types of favorable structural settings.

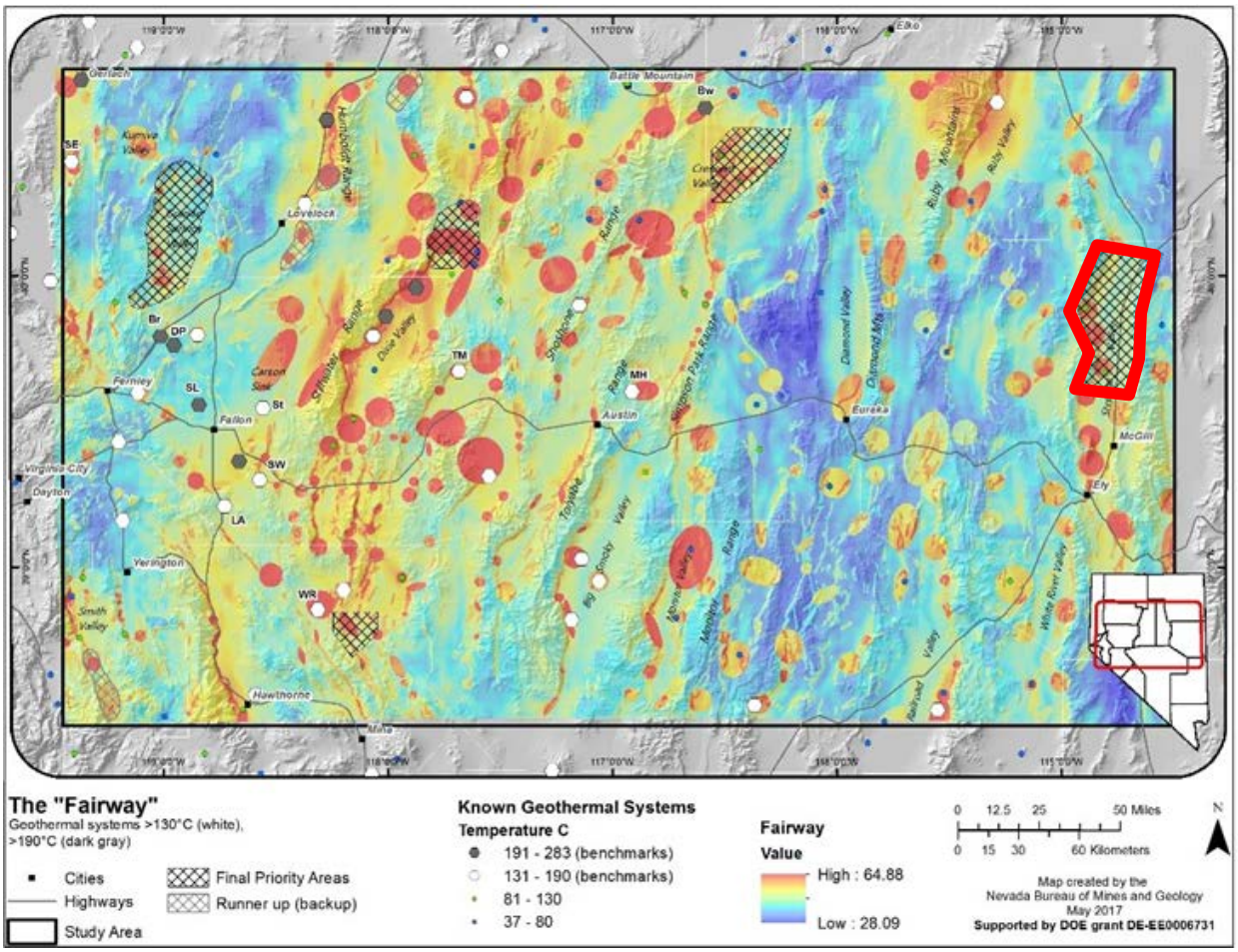

Figure 1: Location of the Steptoe Valley study area (red outline) relative to the initial Nevada play fairway study area (Faulds et al., 2015a). The five areas selected for detailed study during the course of the Nevada play fairway project are shown in black diagonal crosshatch.

The purpose of conducting the detailed field studies were to both increase the level of detail and also increase the quality or confidence in the data, as possible, of the respective inputs in this play fairway analysis (Figure 2). For example, the Quaternary fault layer that was used in the initial regional play fairway analysis is a fault layer that was mapped and compiled at 1:250,000 scale. In contrast, the updated geologic mapping in this study built a new fault layer at 1:24,000 scale. Table 2 shows which data categories listed in Figure 2 received updates and what activities contributed to the data updates. The two parameters that were not updated from the regional-scale data include earthquake seismicity and

geodetic strain rate. Steptoe Valley was one of the five detailed study areas that received a local area update of the heat source model (Figure 2). All other study areas that were a part of the greater Nevada play fairway project used the same Great Basin-wide conductive heat flow model, which has less detail than the one produced for Steptoe Valley. The specific computational process used to integrate the data in this play fairway analysis are covered in previous publications and are not repeated in detail in this paper (Faulds et al., 2015a, b, 2016a, b, c). This paper focuses on the results of the detailed study of the Steptoe Valley study area.

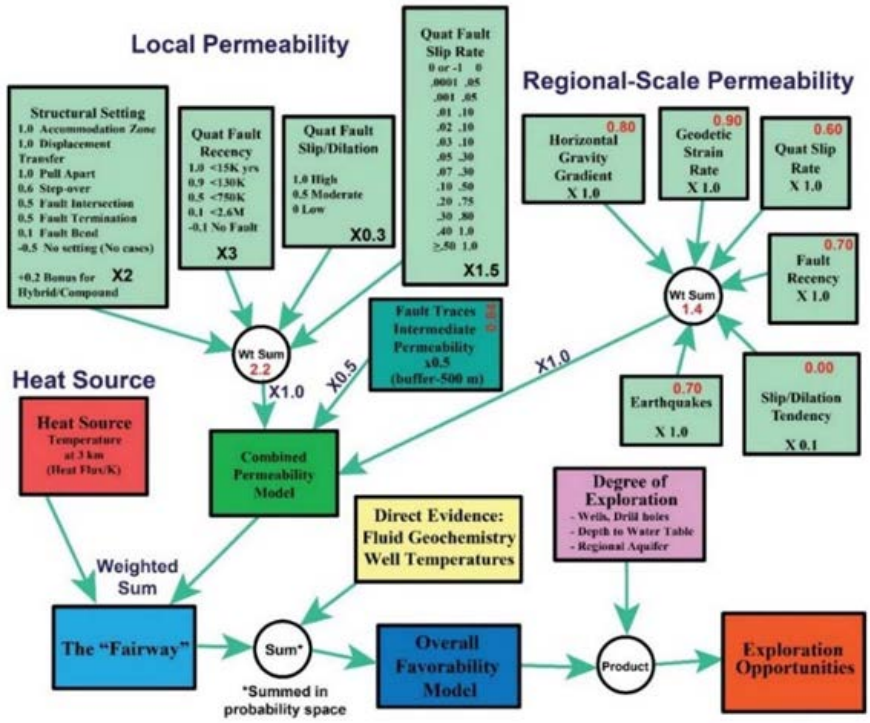

Figure 2. Workflow diagram showing the data inputs and weighting parameters of the data for this play fairway analysis methodology (Faulds et al., 2015a).

Table 1. Left Column: Updated data inputs for local Steptoe Valley play fairway analysis (Figure 2) in the column on the left. Right Column: Field activities and modeling implemented in this study to produce or update the datasets in the in the column on the left.

Data	Activity
Structural Setting	Geologic Mapping, Geologic Well Log Analysis, 2D Seismic Line Interpretation, Gravity Studies, 3D Geologic Modeling
Quaternary Fault Recency	Geologic Mapping
Quaternary Fault Slip Rate	Geologic Mapping
Quaternary Fault Slip and Dilation Tendency	Geologic Mapping, 3D Geologic Modeling, Structural Analysis
Horizontal Gravity Gradient	Gravity Survey and Modeling
Heat Source	3D Heat Flow Modeling, 3D Geologic Modeling, Gravity Modeling, Geologic Well Log Analysis, Analysis of Thermal Conductivity from Cuttings
Direct Evidence	Geochemistry Sampling and Modeling, Spring Temperature Measurements, Geologic Mapping (search for sinter, travertine, or alteration)

2. Geologic Setting and Geothermal Exploration History

Steptoe Valley is an elongate north-trending late Cenozoic west-tilted half graben in eastern Nevada, bounded on the west by the Cherry Creek and Egan Ranges and on the east by the Schell Creek Range (Figures 1 and 3). The study area boundaries were selected to include several highly favorable areas identified in the initial regional study and also where substantial subsurface data were available, including existing borehole data and 2D seismic reflection profiles that can be used to help with deciphering the stratigraphic and structural framework. The study area contains two known hot springs, Monte Neva Hot Springs (79 °C) and Cherry Creek Hot Springs (61 °C), both associated with normal fault step-overs (Faulds and Hinz, 2015; Hinz et al., 2015).

Hunt Oil Company drilled ~50 temperature gradient holes (TGHs) and two deep geothermal wells in the basin in the 1970s (Chovanec, 2003). A few holes reported some lost circulation zones, but the temperature gradients were largely conductive with normal gradients, and no major convective resource was encountered. However, much of the basin has not been explored, including key structural target areas.

Steptoe Valley has also been one of the primary focus areas for studies of geothermal resources in deep sedimentary basins, with elevated temperatures initially documented during oil and gas well drilling (Allis, et al., 2011; 2012; Kirby, 2012; Allis and Moore, 2014; Gwynn et al., 2014). These studies suggest large, untapped geothermal resources exist within stratigraphic horizons at depth in Cenozoic basins in eastern Nevada and western Utah, including this portion of Steptoe Valley. These studies show a high heat flow of 90 to 100 mW/m^2 corresponding to temperatures of 170 to 230°C at ~3 km depth.

3. Geologic Investigations – Permeability Mapping

Geologic investigations included: (1) detailed and reconnaissance geologic mapping of bedrock stratigraphy and structure, and Quaternary deposits, (2) detailed mapping of any active and inactive surficial geothermal manifestations, (4) analysis of the geometry and kinematics of fault systems and assessment of the stress field, (5) Quaternary fault analysis (recency and slip rate), and (6) logging of available cuttings and core.

3.1. Quaternary Fault Mapping and Characterization

Geologic mapping and evaluation of 1:24,000 scale stereo air photos were used to map surficial deposits and Quaternary fault scarps across the study area. Overall, the distribution of Quaternary faults is broadly similar between the new more detailed mapping and the previous existing mapping (Figure 3). The differences lie within the accuracy and detail of steps and bends in the range-front fault and also the overall location of faults on the east side of the basin. The updated mapping along the range-front has shifted many fault segments 250 to 500 m laterally and has identified many previously unmapped fault strands. One example of the greater detail is a newly identified ~200 m-wide-left step at Cherry Creek Hot Springs (inset in Figure 3), at a scale similar to that associated with the Bradys geothermal system (Faulds et al., 2010). On the east side of the basin, previously mapped scarps could not be confirmed with the segments shown by blue lines in Figure 3. However, a new set of scarps was identified cutting a young (Qfy) fan sequence across the basin to the northeast of Cherry Creek Hot Springs.

Based on a published paleoseismic study, most recent rupture of the range-front fault system is late Pleistocene (Koehler and Wesnousky, 2011). The observations collected during mapping in this study are consistent with the published study on recency of faulting. Slip rates for all major singular strands of the range-front fault are 0.03 mm/yr (determined in Faulds et al., 2015a). Locally, the range-front fault system forks into a number of splays in step-overs (e.g. near Monte Neva Hot Springs) with strain distributed across the splays and respectively lower slip rates per fault strand, a characteristic that remains

unchanged from the initial play fairway analysis.

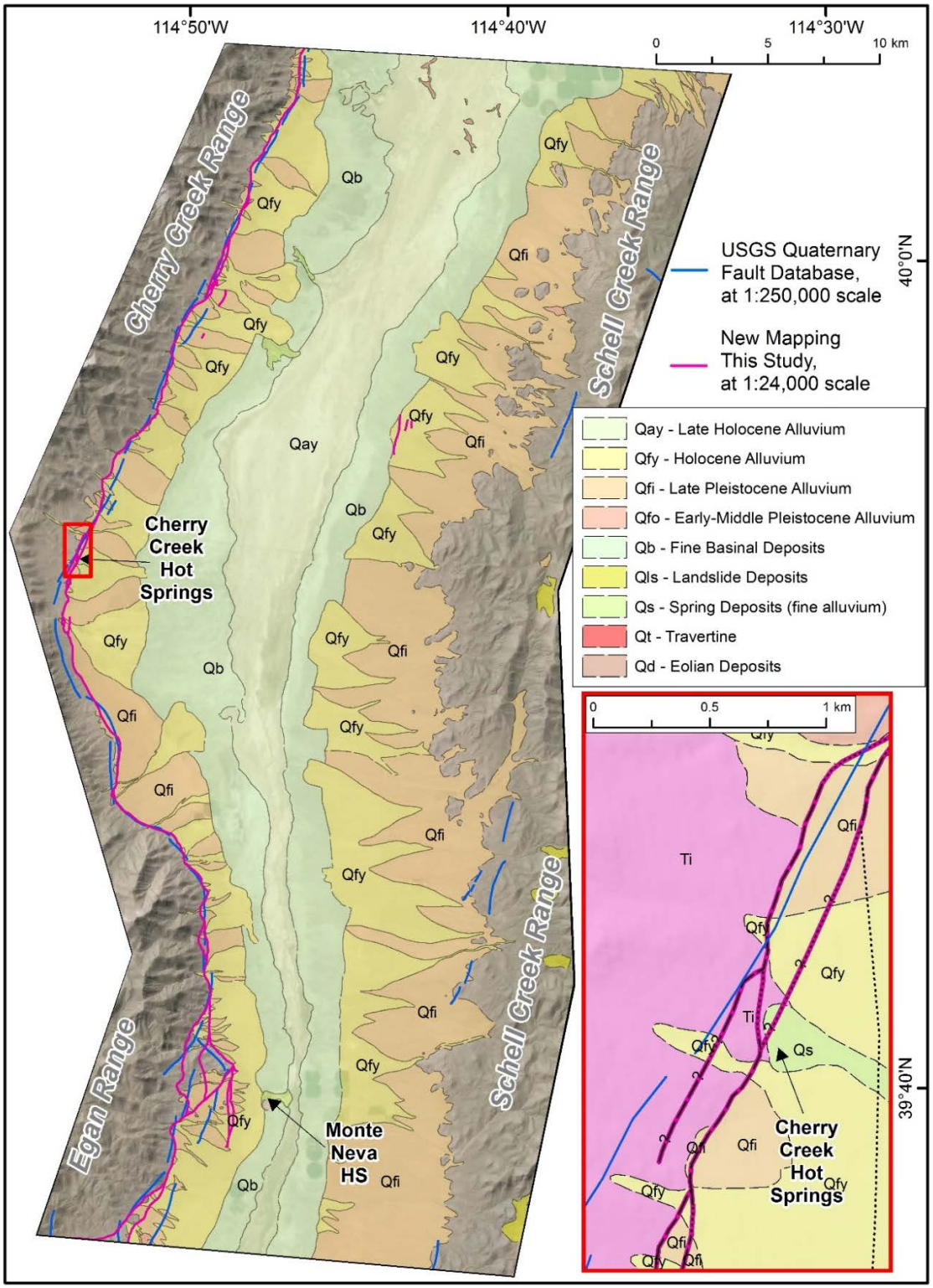

Figure 3. Quaternary surficial deposits and comparison of Quaternary fault mapping generations: blue lines are 1:250,000 scale Quaternary fault traces, data that were available to the initial regional play fairway analysis (Faulds et al., 2015a), and magenta lines are new fault traces generated from mapping in this study. Red rectangle on main map corresponds to inset map for the Cherry Creek Hot Springs area.

3.2. Geologic Mapping, Geophysical Modeling, and Reevaluation of Structural Settings

The trace of the range-front fault is clearly defined by late Pleistocene fault scarps that displace the surfaces of the Qfi fans or generate faulted contacts between Qfi deposits and the bedrock units of the adjacent mountain range. Intrabasinal faults may also be Quaternary and contribute to geothermal activity (e.g., Soda Lake or Stillwater), but surface expressions of these faults are buried by younger deposits, including Qay, Qb, or Qfy. To revise the delineation of structural settings for the updated play fairway analysis in this study (Figure 2), a comprehensive map of late Cenozoic faults was constructed through new geologic mapping, integration of existing mapping, review of cuttings and lithologic logs from existing wells, gravity modeling, interpretation of 2D reflection seismic lines, and 3D geologic modeling. The process of building this map (Figure 4) is described below.

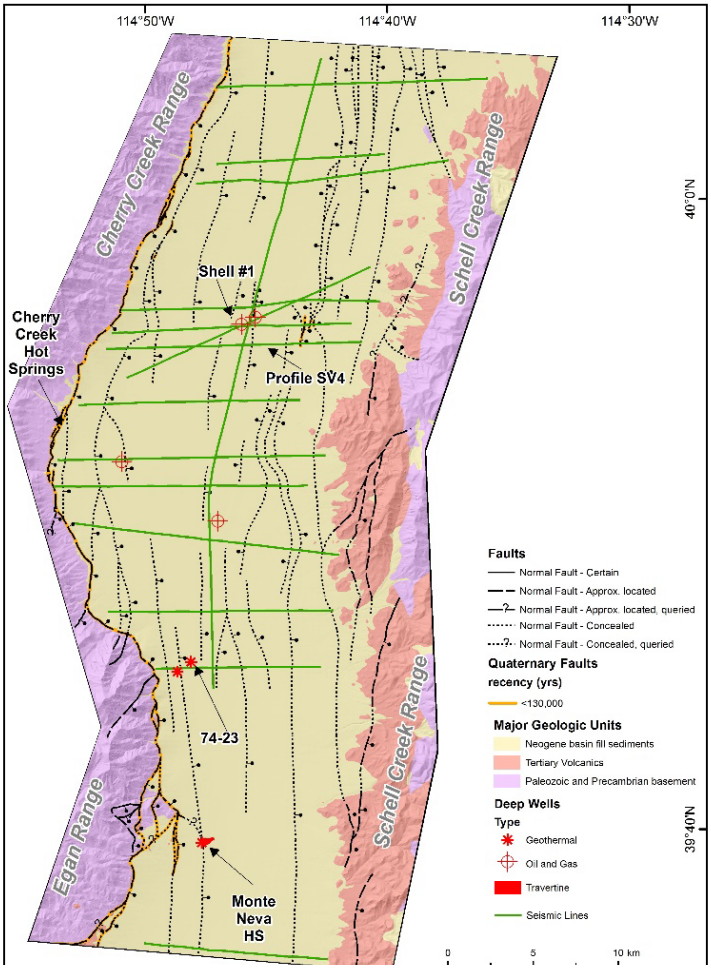

Figure 4. Updated geologic mapping of the study area, including data from field mapping, 2D seismic line interpretation, well data, gravity modeling, and 3D geologic mapping.

3.2.1. Geologic Mapping

New field mapping was conducted at 1:24,000 scale along much of the range-front fault system on the west side of the basin and merged with existing mapping of the bedrock (Fritz, 1968; Hose et al., 1976) to produce a new geologic map of the study area consisting of Tertiary, Paleozoic, and Precambrian units. This mapping has identified where some splays from the range-front fault system continue into the ranges and also fault offsets of the Tertiary volcanic and sedimentary strata on the east side of the basin. Overall, the faults are dominantly N-S striking with down-to-east normal displacement (Figure 4).

The stratigraphy in Figure 4 is simplified to show three primary units (Neogene basin-fill sediments, Tertiary volcanic rocks, and Paleozoic and Proterozoic basement. The Paleozoic strata are dominantly carbonates, and the Proterozoic are dominantly metasediments (Fritz, 1968; Hose et al., 1976; mapping this study). The Paleozoic and Precambrian basement unit in Figure 3 also contains some Tertiary and older plutons that are lumped at this map scale. The reasons for lumping the stratigraphy into 3 units was for the effectiveness of mapping intrabasinal faults. Core was not available from the existing wells in the basin, and it is difficult to determine the differences between the respective Paleozoic carbonate strata from chips only. Furthermore, distinguishing the three main units (basins sediments, volcanics, and basement rocks) is about the limit of the resolution of the existing reflection seismic data. Therefore, to generate a full 3D geologic map of the late Cenozoic fault architecture, it was most effective to lump the stratigraphy into three primary units.

3.2.1. Gravity Surveys and Modeling

A total of 287 new gravity stations were acquired during the 2016 field season and were integrated with 1762 existing gravity stations (Figure 5). Most of the new stations were placed along the traces of 2D seismic reflection profiles to provide maximum control for modeling along these cross sections. Separate to providing a reference for 2D seismic interpretation, the total suite of gravity data were used to generate a new horizontal gravity gradient grid for use as one of the inputs in the local-scale play fairway analysis (Figure 2).

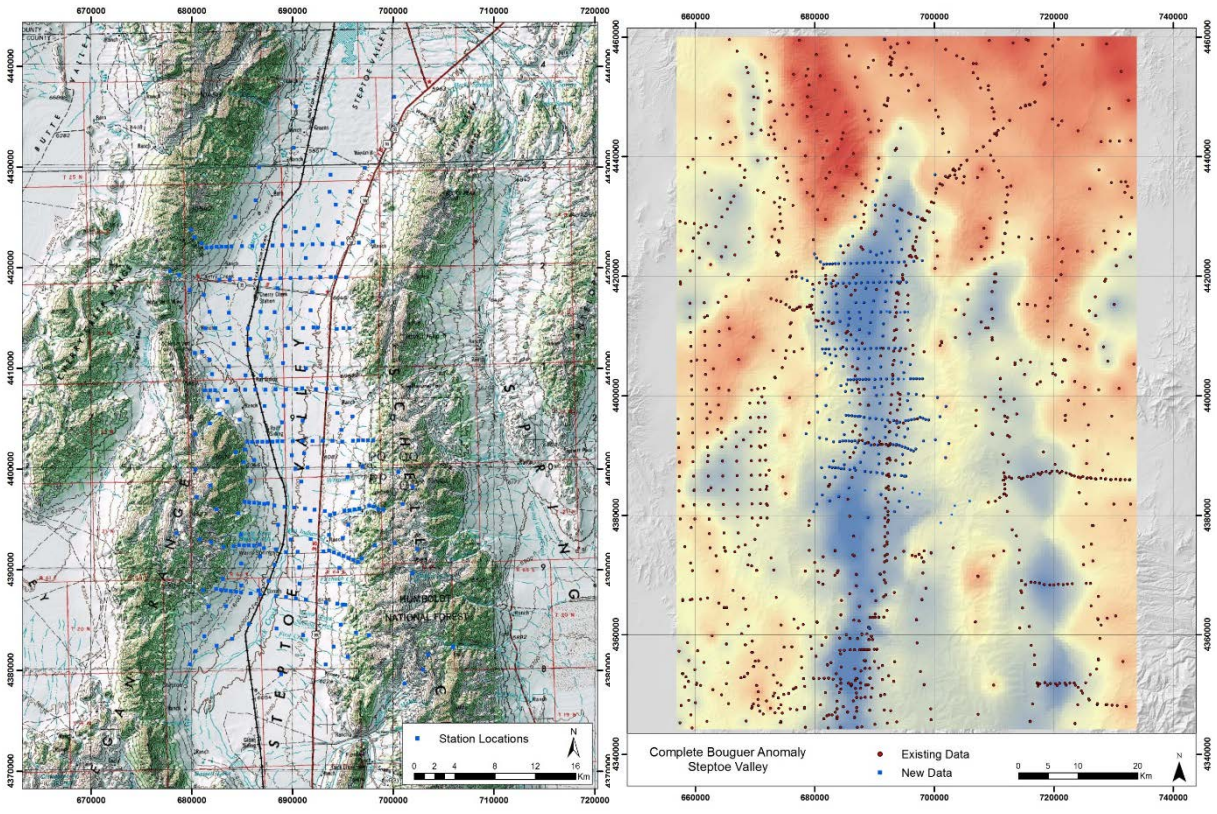

Figure 5. Map of new and existing stations on a topo map (left) and on a complete Bouguer anomaly (right).

Simplified 2D gravity models of six transects in the Steptoe Study area were generated using a variable thickness sedimentary layer overlying Tertiary volcanic rocks and older rock units (e.g., Figure 6). The gravity anomaly values along the transect were adjusted for regional effects using low-order polynomials and subsequently modeled using the semi-automated Marquardt inversion code (SAKI) of Webring

(1985). The sediment and bedrock density contrasts were held constant for specific interval depths (for sediment layers) and based on values from local geological information, samples, and drill logs of equivalent geographic areas containing deep sedimentary basins. A density-depth profile was developed using deep well data, and densities were assigned in 500 m intervals for the basin fill as follows: 2.0, 2.16, 2.235, 2.31, 2.385, and 2.395 g/cm^3. Tertiary volcanic rocks and older rock units for the Steptoe study area were all assigned a density value of 2.67 g/cm^3.

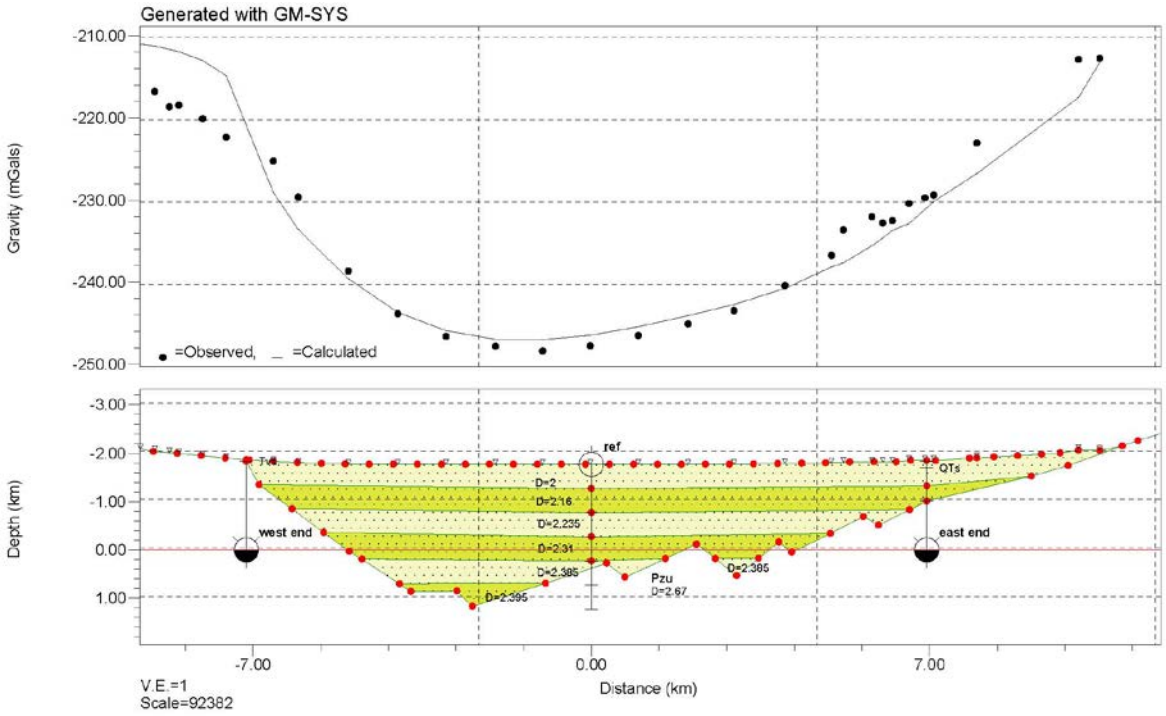

Figure 6. Gravity profile modeling along profile SV4.

Bedrock outcrops on the margins of the valley, lithologic information from drill logs (where applicable and trusted), and interpreted seismic profiles were used as depth-to-bedrock control points for the model to check layer density picks. All profiles are somewhat consistent in general geometry. The profiles show an asymmetric basin comprised of steeply-dipping interfaces and deeper bedrock on the west side of the half graben compared to more gently-dipping interfaces on the east side of the basin.

3.2.2. Seismic Reflection

Nearly 200 km of seismic reflection data, originally acquired in the early 1970s to mid-1980s, were interpreted. Plots of seismic cross sections were combined with locations of faults and lithological boundaries known from surface mapping, well information, and gravity model profiles. Two different workflows were used for interpretation of these data. If only a scanned paper image was available for a particular line, a time domain flow was pursued. If usable SEGY files were available, a depth domain flow was implemented. For the time domain flow, if gravity derived depths to formation boundaries were available, they were converted from depth to time. Similarly, if nearby well data were available, formation tops from these wells were converted from depth to time, which were plotted on top of the scanned seismic profile. These profiles were then interpreted for a limited number of faults and lithologies on the time domain images. The interpretation was then digitized, and the digitized points converted from time to depth. If usable SEGY files were available, a depth domain approach was followed. The seismic traces were first converted from time to depth. Available gravity and well data were then incorporated into interpretation of the depth domain traces. An example of one of the interpreted profiles is shown in

Figure 7.

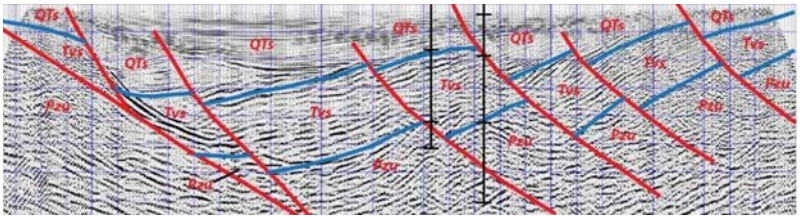

Figure 7. E-W (looking north), interpreted seismic reflection profile (SV4) with local well control. Pzu, Paleozoic sedimentary rocks; other unit names same as in Figure 4. Location also shown in Figure 4. Seismic data owned or controlled by Seismic Exchange, Inc.; interpretation is that of the University of Nevada, Reno.

3.2.3. 3D Geologic Mapping

3D geologic mapping was employed to integrate the geologic map data, well data, and 2D seismic reflection profiles to map the intrabasinal fault architecture. The results of the 3D mapping were used to update the 2D fault map and provide inputs into the 3D conductive heat transfer model. Established methods for 3D geologic mapping (Siler et al., 2016a, b; 2019a, b) and EarthVision software were utilized.

Lithologic logs from 25 wells, geologic map data, 16 cross-sections including data from 14 seismic reflection profiles (Figure 4), and depth to basement modeled from gravity data were synthesized into a 3D geologic map of the Steptoe Valley study area. The Steptoe 3D map contains three stratigraphic units, undivided basement, Tertiary volcanic rocks, and Quaternary/Tertiary sediments (Figure 8). The 3D map reveals the anatomy of the basin, including a broad, gently west-tilted half graben bounded by a major moderately east-dipping range-front on the west and cut by several, relatively minor northerly striking intrabasinal faults. The 3D geologic map constrains the geometry of several structural discontinuities that may be important sites of permeability and fluid flow. Monte Neva Hot Springs occupies a ~2.5 km-wide left-step in the range-front fault (Figures 4 and 8). Several additional steps and bends occur farther north, including one associated with the Cherry Creek hot springs.

Figure 8 (following page). Perspective views of a portion of the Steptoe 3D geologic map looking NNW (top) and NW (middle), and a perspective view of slip tendency calculated along faults in the Steptoe 3D geologic map looking NNW (bottom). Several of the seismic reflection profiles and 2D geologic cross-sections that were used to constrain the 3D geologic relationships are shown protruding from the 3D map on top. Lithologic units, undivided Paleozoic basement (Pzu), Tertiary volcanic rocks in blue (Tv), and Neogene sedimentary rocks (QTs) are shown in green, blue, and yellow respectively. Faults are shown as gray planes and as red lines in section view. Monte Neva Hot Springs is shown with the red dot at a left step-over between a relatively large-offset intrabasinal fault and the range-front fault in the maps at the top and middle. Favorable steps and bends in the range-front fault system are circled in red in the map at the top.

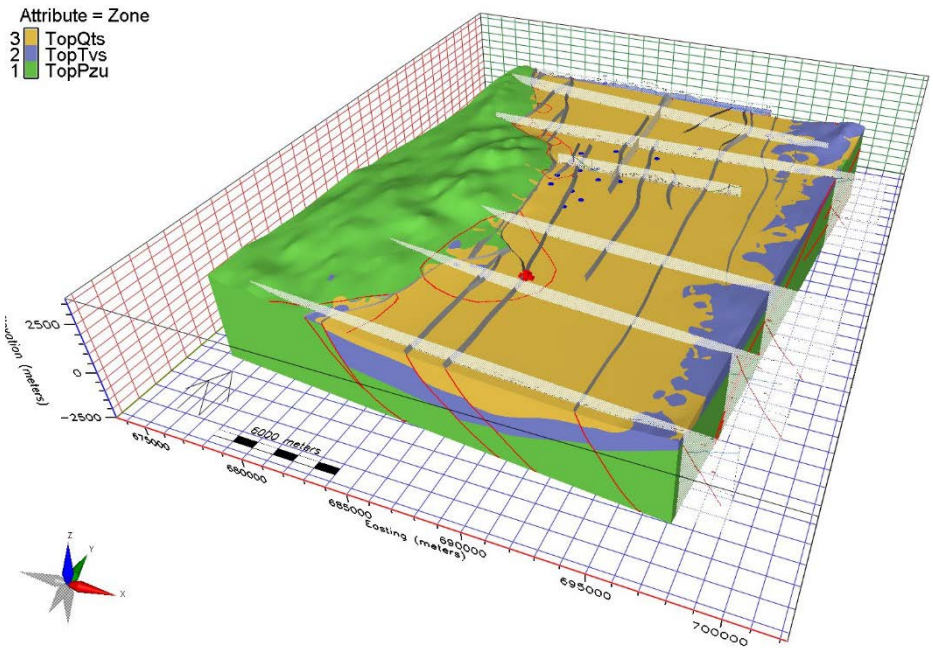
Attribute = Zone
3 TopQts
2 TopTvs
1 TopPzu
2500
0
−2500
Elevation (meters)
6000 meters
675000
680000
685000
690000
695000
700000
Easting (meters)

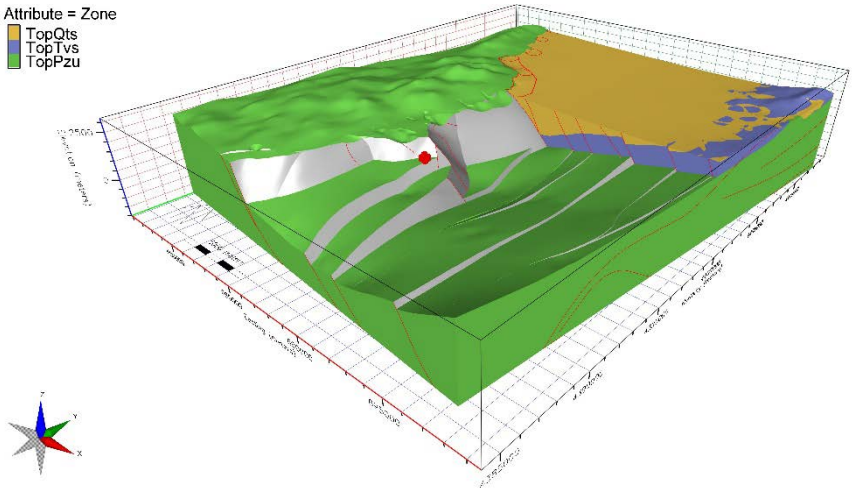
Attribute = Zone
TopQts
TopTvs
TopPzu

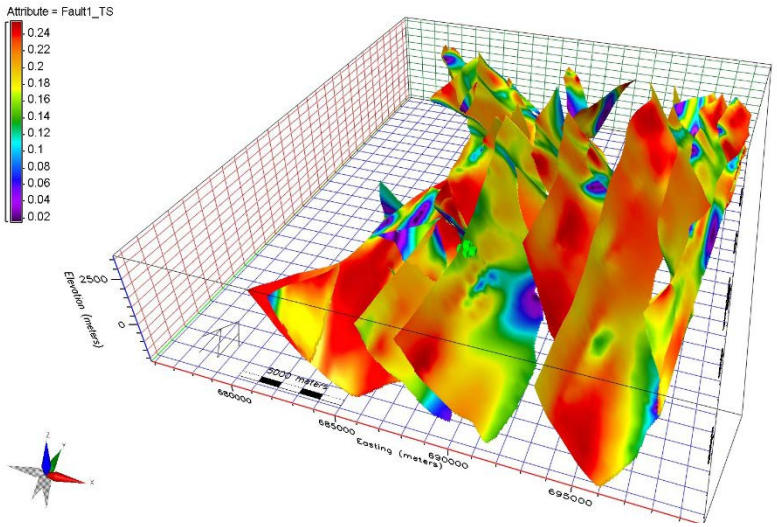
Attribute = Fault1_TS
0.24
0.22
0.2
0.18
0.16
0.14
0.12
0.1
0.08
0.06
0.04
0.02
2500
0
Elevation (meters)
5000 meters
680000
685000
690000
695000
Easting (meters)

3.2.4 Stress Field Determination and Slip and Dilation Tendency

For slip and dilation tendency analysis (e.g. Morris et al., 1996; Ferrill et al., 1999), we assumed a normal faulting stress regime with a minimum horizontal stress (S_{hmin}) direction of 117°, both of which are consistent with regional trends (Heidbach et al., 2016). Under these stress conditions 60°-dipping NNE-striking faults have the highest slip tendency, whereas more steeply-dipping NNE-striking faults have the highest dilation tendency (Figure 8). The predominantly NNE-striking fault system in Steptoe Valley is generally well oriented for both slip and dilation, including at both Cherry Creek and Monte Neva Hot Springs.

3.2.5 Reevaluation of Structural Settings

Twelve favorable structural settings were defined from the new 2D and 3D geologic map (Figure 9). These include seven normal fault step-overs and five fault intersections. The largest and most complex favorable settings include the step-over associated with Monte Neva Hot Springs and a second step-over southwest of Monte Neva. Another key step-over associated with Cherry Creek Hot Springs is just 200 m wide, only slightly narrower than the step-over associated with Bradys Hot Springs (Faulds et al., 2010, 2017; Siler et al., 2016b). Notably, all three step-overs identified above lack continuous Quaternary scarps, indicating that these structures are acting as key arrest zones during earthquake ruptures and may reside in areas of elevated coulomb stresses (e.g. Siler et al., 2018).

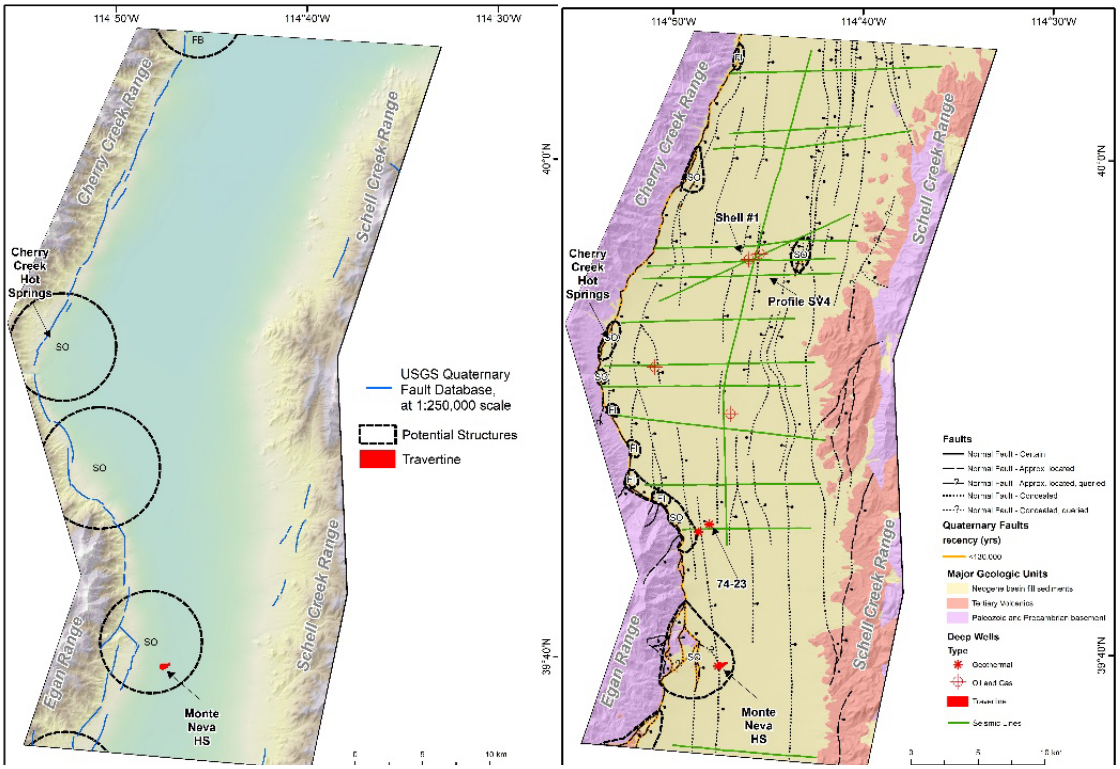

Figure 9. Left: Previous structural target areas before new detailed studies reported in this paper. Right: Updated structural target areas based on new 2D and 3D geologic mapping.

4. Heat Flow Modeling

A 3D conductive heat transfer model using a finite-element modeling program (COMSOL Multiphysics 4.4) was carried out for the Steptoe Valley study area using standard techniques (Edwards, 2013). The Steptoe 3D thermal model framework is based on a simplified, regional- scale mesh of cells (bedrock or basin fill) with an upper and lower geologic boundary (Figure 10a). The interface between basin-fill sedimentary units and Tertiary volcanic rocks and older rock units is derived from the new 3D geologic map. Model parameters include thermal conductivity of the physical layers and basal heat flux. The range of basal heat flux is chosen according to revised calculations as well as previous studies (Gwynn et al., 2014) of logged and extrapolated temperature gradients of the exploration wells in the area. Thermal conductivity values are based on laboratory measurements of 40 samples of Steptoe Valley well cuttings. The thermal conductivity values were then corrected for "in-situ" porosity estimated from downhole well logs. Modeled thermal conductivity values selected for basin fill and bedrock are 1.6 and 3.4 W/mK, respectively. Three thermal models were run using the basal heat flux parameters of 90, 100, and 110 mW/m^2, which are invariant with respect to time.

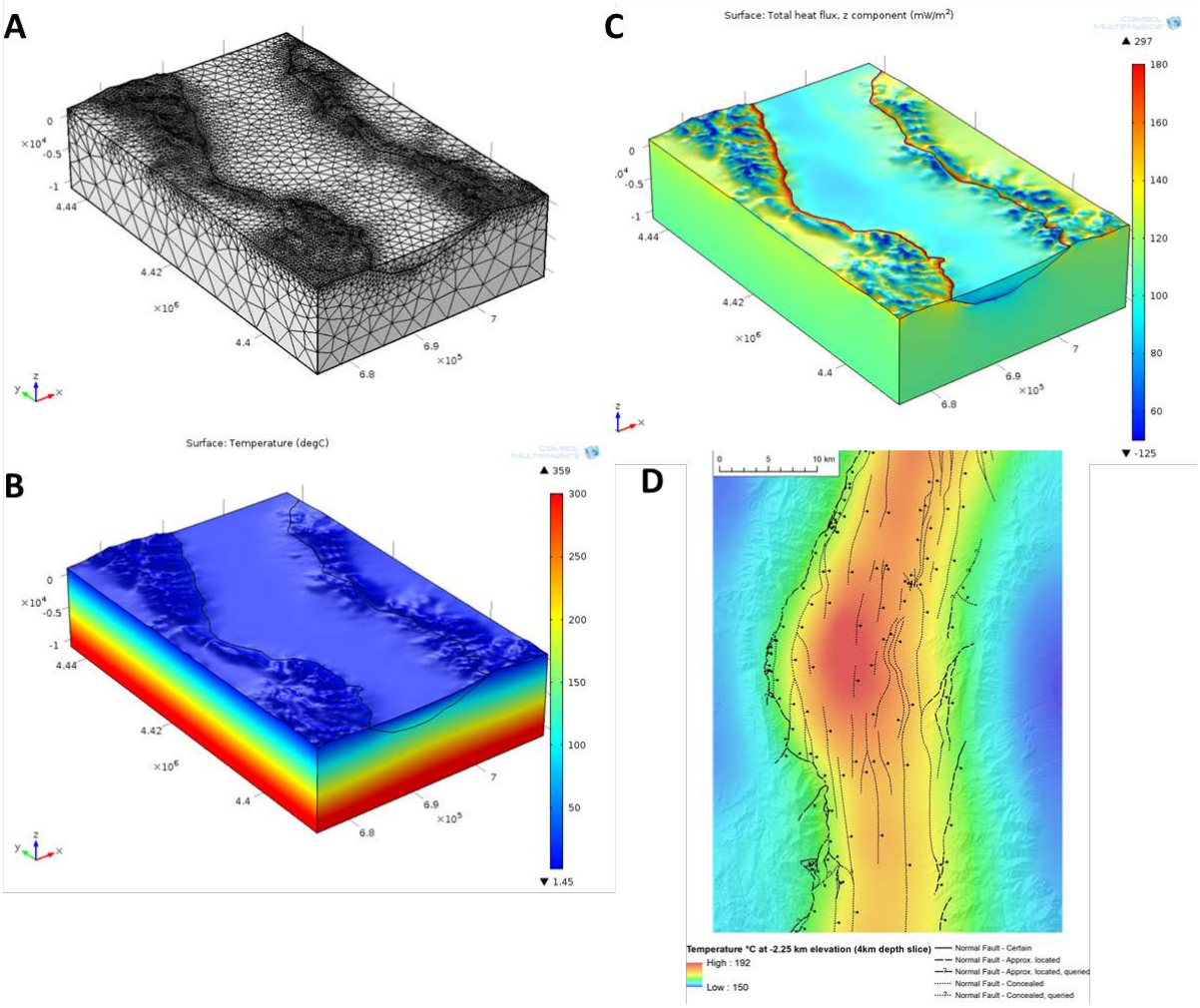

Figure 10. (A) Heat transfer modeling grid. (B) Resulting temperature gradient model. (C) Surface heat flux. (D) Horizontal slice through temperature model at -2.25 km elevation.

Model outputs for each of the basal flux conditions consist of surface heat flow followed by temperature slices generated for 6 horizons starting from a reference elevation of 1750 m and down to 5 km depth below the reference. Temperature gradually increases with depth and are slightly elevated below the bottom of the basin due to thermal "blanketing" effects of low-conductivity basin fill (Figure 10b, d). Note that in a purely conductive model, heat will flow along a preferred pathway that has the highest thermal conductivities and least amount of insulative covering. In this model, the preferred flow paths are through the basement along the boundary of the basin fill (Figure 10c). The temperature field is continuous, whereas heat flow and thermal conductivity are discontinuous across the basin fill/basement boundary (known as heat-flow refraction). For comparison, the older heat model used for the regional play fairway study (Faulds et al., 2015a), generated by Dave Blackwell with regional input on basin depths, is very similar to the new model temperature ranges at 3 km, though with much poorer resolution.

5. Updated Play Fairway Analysis

The detailed geologic and geophysical studies supported key updates for the fairway model (Figure 11). Greater detail in the 3D geologic mapping allowed for the larger target areas to be modified to fit better defined targets and also facilitated the identification of new smaller targets. Identification of the smaller structural target areas was not possible with the previously available geologic map detail.

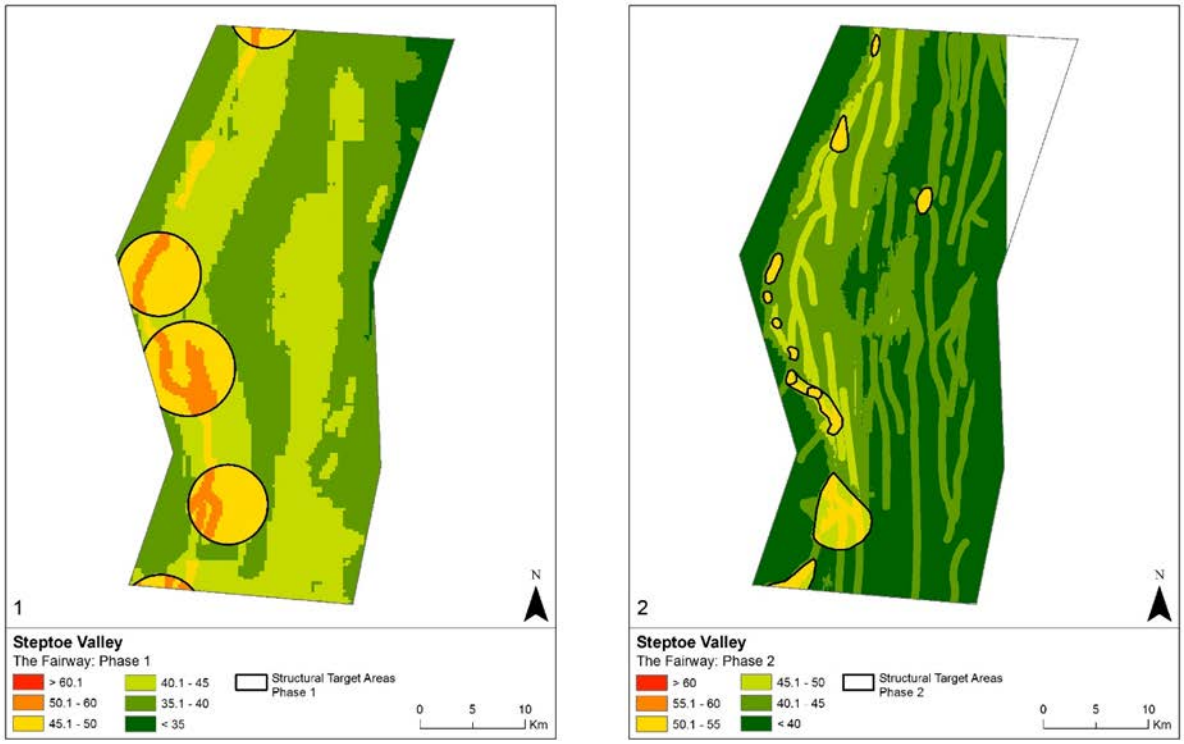

Figure 11. Left: Previous play fairway model (Faulds et al., 2016). Right: Updated play fairway analysis.

6. Direct Evidence: Temperature, Geochemistry, and Surficial Geothermal Features

Direct evidence confirming the presence of thermal anomalies in Steptoe Valley includes measured temperatures in springs and wells in the valley, and chemical geothermometry estimates. Eighteen chemical analyses from springs and wells are available in the study area, including 17 historical samples and one sample each from gray literature and this study (Table 2). All samples are classified as bicarbonate fluids (Figure 12), and typically have total dissolved solids (TDS) less than 500 ppm.

Samples from Cherry Creek Hot Springs and well 37-23 have higher TDS and have some chemical similarities (Figure 13) that could suggest similar fluid origins. Monte Neva Hot Springs has the hottest surface discharge of fluids in the area at 79 °C, and is associated with a 0.28 km^2 travertine spring mound with multiple active spring emanation points on and around the edges of the mound (Figure 14). Cherry Creek Hot Springs has a maximum measured temperature of 61 °C and is not associated with any travertine deposition. Other warm springs/wells are present in Steptoe Valley with temperatures over 20 °C, suggesting some mixing with a thermal fluid (Table 2). Temperature measurements were obtained for several of the unnamed springs along the western side of the basin during the geologic mapping efforts however all were cold. Deep wells in this area have measured bottom-hole temperatures of 198-200 °C at 3,306-3566 m depth (Hunt geothermal 74-23 and Shell #1 wells; Figure 14). However, only one has chemistry data, and all have conductive temperature profiles.

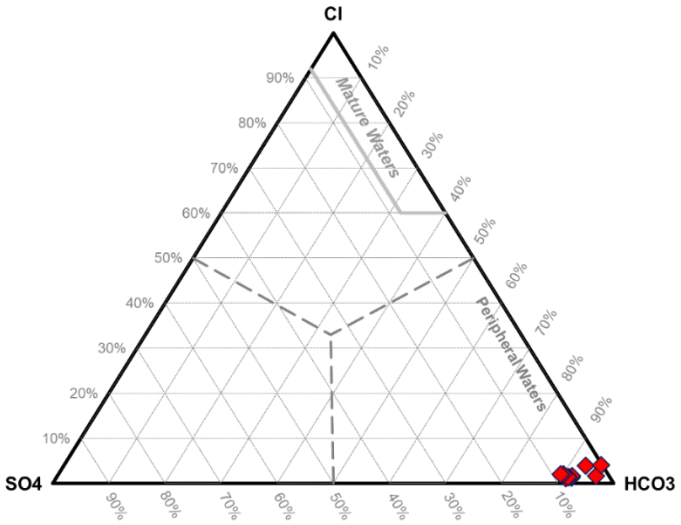

Figure 12: Ternary plot for spring and well water samples in Steptoe Valley: all are bicarbonate-dominated.

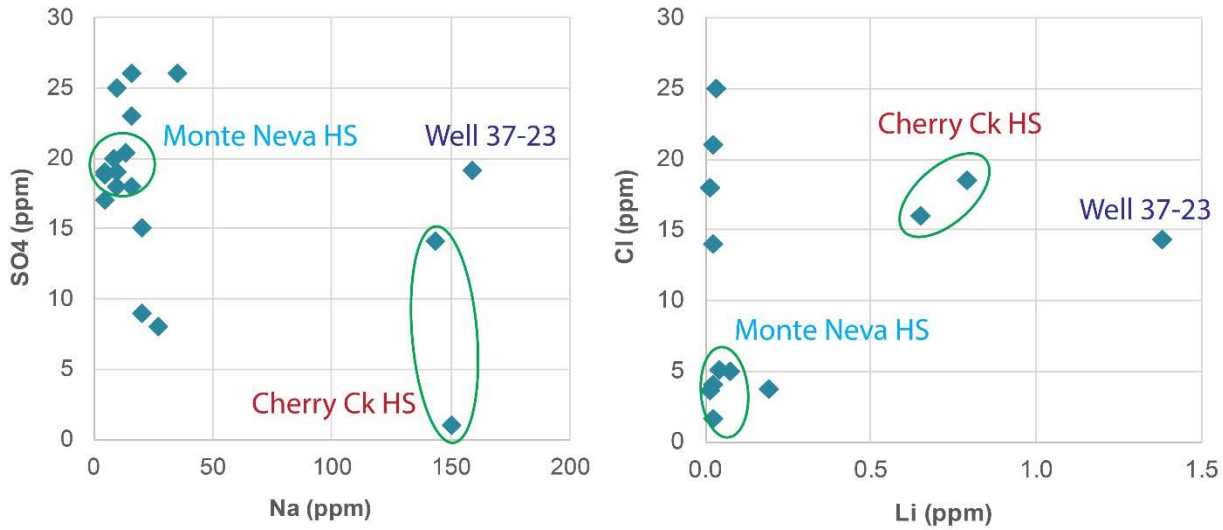

Figure 13: Cross plots illustrating chemical trends for spring and well water samples in Steptoe Valley: Cherry Creek hot springs, and a sample from well 37-23 are distinct from all other samples collected.

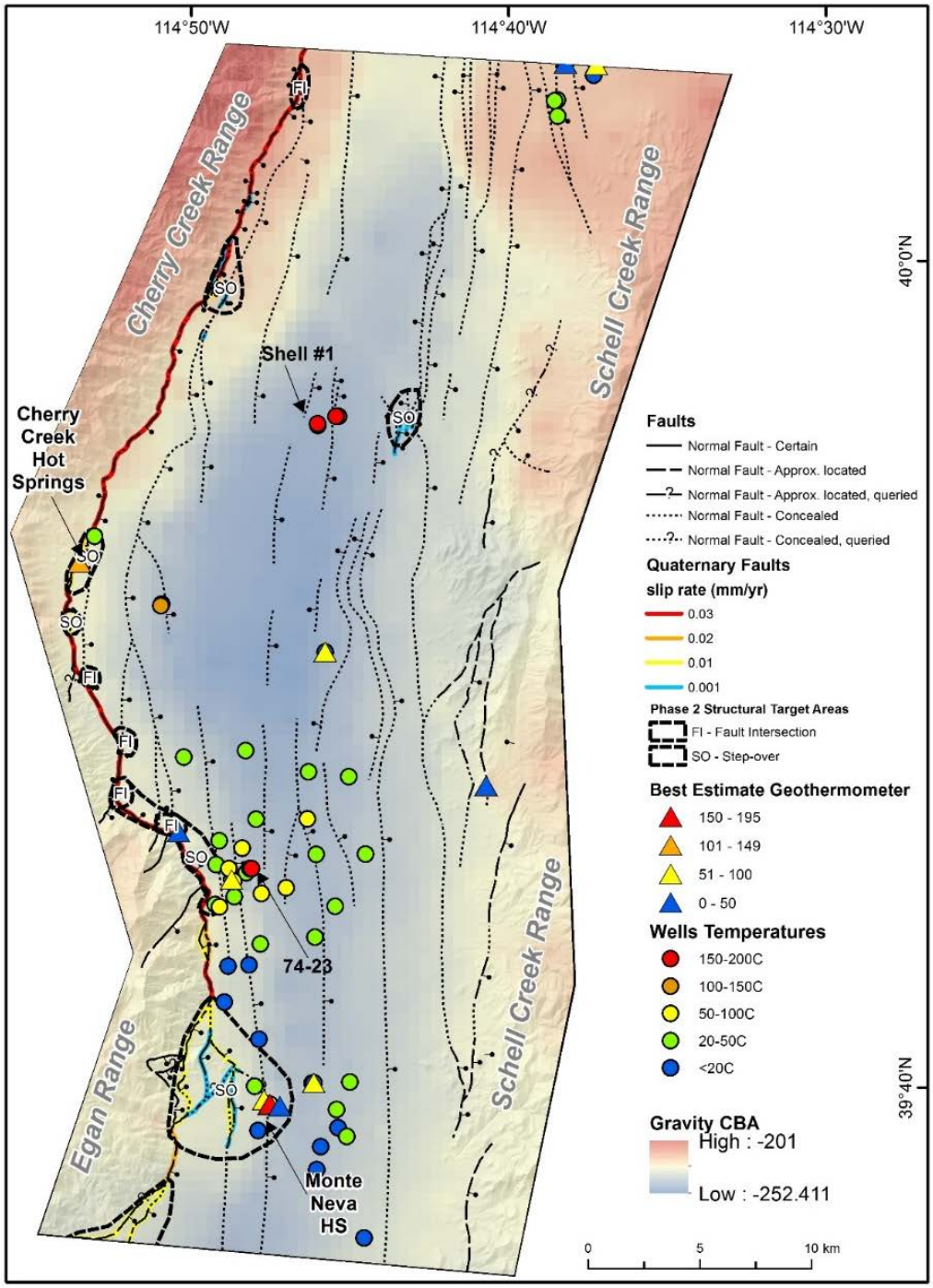

Figure 14. Distribution of wells with water geothermometry and measured temperature data (maximum measured temperature of each well is shown), the structural target areas and late Cenozoic faults on a gravity model (CBA) base draped over a hillshade. Well temperatures are from a broad range of well depths (e.g. TG holes of <150 m deep to petroleum exploration wells > 2 km deep) and cannot be compared relative to each other without the depth data. Wells are shown here to show XY spatial extent of these data coverage.

Traditional cation geothermometry results for the water samples display a wide range of estimated equilibration temperatures (either much lower than measured temperatures, or substantially hotter than measured temperatures (even exceeding the critical point for water (>374 °C), thus are not considered reliable (Table 2). This may be as a result of the bicarbonate fluid chemistry: the traditional cation geothermometers are typically most effective when applied to alkali-chloride fluids, where it is assumed that temperature-sensitive equilibrium exchange reactions with the alkali feldspars govern Na and K concentrations. Multiple-component equilibrium geothermometry is likely to be more reliable, as chemical equilibria are calculated for multiple minerals that are expected to be present in the geothermal reservoir. GeoT modeling results for selected springs in Steptoe Valley indicates potential equilibrium temperatures of 180±3 °C at Monte Neva Hot Springs, 136±5 °C at Cherry Creek Hot Springs, and 174±3 °C in well 37-23 (Nic Spycher, *pers. comm*, 2017). Thus, power-capable geothermal systems are likely at all three areas, although the higher temperatures (>180 °C) are more likely to be encountered at ≥ 3 km depth. Conductive temperature gradients of the Hunt wells average ~60 °C/km, suggesting the >180 °C resources in the vicinity of those wells and at Monte Neva are at depths of ~3 km. Results at Cherry Creek suggest a shallower, intermediate system that could exploit a lower temperature (~135°C) resource.

Table 2. Summary of conventional geothermometry estimates for spring and wells samples in the study area. All geothermometry estimates in °C.

Site name	Date	Temp (°C)	pH	Li (ppm)	Na (ppm)	K (ppm)	Ca (ppm)	Mg (ppm)	SiO2 (ppm)	B (ppm)	Cl (ppm)	F (ppm)	SO4 (ppm)	HCO3 (ppm)	TDS (ppm)
Central Steptoe Valley															
Borchert John Warm Spring	8/25/1978	18	7.8		4.80	1.00	49.0	21.0	11.0		4.00	0.10	17.0	180	288
LAP&W Well 1	9/16/1982	18.4	8.2	0.04	16.0	4.40	49.0	10.0	58.0	0.040	5.10	0.60	18.0		161
Schellbourne Springs		24.6	8.29		4.30	1.40	56.0	17.0	23.0		3.60	0.27	19.0	232	357
Schellbourne Springs	5/1/1980	24.6	8.29	0.01	4.28	1.38	56.4	16.7	22.8		3.58	0.24	18.8	232	356
Well 37-23	1979	90.6	7.19	1.38	159	41.4	60.4	27.2	51.8	0.8	14.3	3.53	19.1	805	1184
Cherry Creek (Western Steptoe Valley)															
Cherry Creek Hot Springs	4/21/1974	61		0.65	150	4.80	12.0	0.3	105	0.350	16.0	1.20	1.00	376	667
Cherry Creek Hot Springs	6/25/2002	60.5		0.79	143	7.10	34.9	0.3	101	0.388	18.5	13.1	14.1	432	765
East of Steptoe Valley															
Warm Well, D Henriod Ranch	7/27/1983	28.2	8	0.02	20.0	9.50	26.0	8.7	71.0		21.0	0.40	9.0		166
Monte Neva area															
Monte Neva Hot Springs	2/17/2017	78.2	7.4	nd	16.0	5.90	68.0	19.0	50.0	nd	3.30	1.10	23.0	260	446
Monte Neva Hot Springs	4/21/1974	79		0.07	16.0	5.60	63.0	21.0	52.0	0.040	5.00	1.00	26.0	303	493
Monte Neva Hot Springs	6/25/2002	77.6		0.19	13.5	7.60	53.4	18.7	51.1	0.100	3.70	0.80	20.4	269	438
NWIS Well 179 N21 E64 19BDAD1	6/14/1984	14	8	0.02	35.0	3.80	37.0	5.3	44.0		14.0	0.40	26.0		166
Northern Steptoe Valley															
NWIS Well 179 N26 E65 34DABA2	7/27/1983	14.8	8	0.03	20.0	6.50	41.0	9.7	60.0		25.0	0.20	15.0		177
Warm Well - Collar and Elbow Spring	11/3/1940	22	7.74		8.40	4.00	49.0	17.0	24.0		5.10	0.33	20.0	226	354
Southern Steptoe Valley															
Campbell Ranch Springs	7/15/1981	24	7.7	0.02	9.30	3.60	52.0	20.0	19.0	0.050	4.10	0.30	19.0		127
Campbell Ranch Springs	8/25/1978	24	7.3		9.30	3.40	51.0	21.0	19.0		4.40	0.40	18.0	250	377
NWIS Well 179 N19 E63 26CCB 1	7/26/1983	14	8.1	0.02	27.0	8.30	23.0	14.0	58.0		1.60	0.30	8.00		140
NWIS Well 179 N20 E64 17DD 1	6/14/1984	14.5	8	0.01	9.40	3.10	53.0	14.0	33.0		18.0	0.10	25.0		156

The presence of hydrothermal alteration can indicate geothermal activity: it is noted in several places along the range-front fault on the western edge of Steptoe Valley, but is attributed to Tertiary magmatism rather than recent hydrothermal activity.

9. Conclusions and Remaining Data Uncertainties

The detailed geologic and geophysical studies supported key updates for the fairway model (Figure 11), the backbone of which is the structural framework and kinematics. The geologic and geophysical updates confirmed the existing overall structural model (west-tilted half graben, bound by a major east-dipping normal fault system on the west), and refined details of the range-front fault architecture and intrabasinal faulting. This resulted in the identification of new and smaller structural targets along the range-front fault system, and one new target in the east-central part of the basin, east of the Shell #1 well. This brought up the total number of structural targets from 5 to 12. Two of these areas are associated with Cherry Creek and Monte Neva Hot Springs, the rest are largely unexplored.

No new hot springs or other active or inactive surficial manifestations were encountered. GeoT modeling of fluids from Cherry Creek and Monte Neva Hot Springs both suggest that power capable (>130 °C) reservoir temperatures are possible. Other structural target areas have similar fairway scores to Cherry Creek and Monte Neva Hot Springs (Figure 11). Temperature gradient drilling at these locations will be needed to confirm if undiscovered blind resources are present.

Although, the new geoscience studies have increased resolution across the study area, uncertainties do remain in the datasets. Lidar data was not available for Steptoe Valley and this would provide additional detail over the mapping that was completed with 1:24,000 scale air photos. In particular, Lidar could help identify additional splays and detail of the range-front fault system and also with identifying Quaternary faulting in the basin (e.g., fault scarps observed in imagery east of Shell #1 well. The historic seismic reflection line data that was used to help map the intrabasinal stratigraphic contacts and faults for 2D and 3D mapping is limited in accuracy, both with time to depth conversion and also with the resolution of picking features. New 2D or 3D seismic reflection data would provide substantial gains in resolving the intrabasinal structural framework and provide. Not all groups of springs around the basin have been sampled or geochemistry or have had temperatures measured. Additional ground could also be covered to explore for fossil spring deposits or alteration associated with the newly identified structural target areas.

8. Acknowledgement

This material is based upon work supported by the U.S. Department of Energy's Office of Energy Efficiency and Renewable Energy (EERE) under the Geothermal Technologies Program and Play Fairway Analysis initiative (award number DE-EE0006731 awarded to Faulds). Drew Siler from the U.S. Geological Survey is acknowledged for completing the detailed 3D geological mapping and the slip and dilation tendency analysis. Lisa Shevenell, retired from ATLAS Geosciences, Inc., is credited for overall management of the geochemical investigations. Nicolas Spycher from LBNL is thanked for conducting the GeoT multiple component equilibrium modeling for three water samples from Steptoe Valley. Alan Ramelli of NBMG, UNR is credited for completing the surficial geologic mapping and Quaternary fault mapping updates.

REFERENCES

Allis, R., and Moore, J, 2014, Can deep stratigraphic reservoirs sustain 100 MW power plants: Geothermal Resources Council Transactions, v. 38, p. 1009 – 1016.

Allis, R., B. Blackett, M. Gwynn, C. Hardwick, J. Moore, C. Morgan, D. Schelling, and D.A. Sprinkel, 2012. Stratigraphic Reservoirs in the Great Basin — The Bridge to Development of Enhanced Geothermal Systems in the U.S. Geothermal Resources Council Transactions 36: 351-358.

Allis, R., J. Moore, B. Blackett, M. Gwynn, S. Kirby, and D. Sprinkel, 2011. "The Potential for Basin- Centered Geothermal Resources in the Great Basin." Geothermal Resources Council Transactions, v. 35, p. 683–688.

Chovanec, Y.M., 2003, Geothermal analysis of Schellbourne, East-Central Nevada, Steptoe Valley [M.S. Thesis]: University of Texas at Arlington, 138 p.

Craig, J.W., 2018, Discovery and analysis of a blind geothermal system in southeastern Gabbs Valley, western Nevada [M.S. Thesis]: University of Nevada, Reno, 111 p.

Craig, J.W., Faulds, J.E., Shevenell, L.A., and Hinz, N.H., 2017, Discovery and analysis of a potential blind geothermal system in southern Gabbs Valley, western NV: Geothermal Resources Council Transactions, v. 41, p. 2258-2264.

Edwards, M. C., 2013, Geothermal resource assessment of the Basin and Range province in western Utah, Salt Lake City, University of Utah, M.S. Thesis, 123 p.

Faulds, J. E., Hinz, N.H., Coolbaugh, M. F., Shevenell, L. A., and Siler D. L, 2016a, The Nevada play fairway project — Phase II: Initial search for new viable geothermal systems in the Great Basin region, western USA: Geothermal Resources Council Transactions, v. 40, p. 535-540.

Faulds, J. E., Hinz, N.H., Coolbaugh, M. F., Shevenell, L. A., Sadowski, A.J., Shevenell, L.A., McConville, E., Craig, J., Sladek, C., and Siler D. L, 2017, Progress report on the Nevada play fairway project: Integrated geological, geochemical, and geophysical analyses of possible new geothermal systems in the Great Basin region: Proceedings, 42nd Workshop on Geothermal Reservoir Engineering, Stanford University, Stanford, California, February 13-15, SGP-TR-212, 11 p.

Faulds, J.E., Coolbaugh, M.F., Benoit, D., Oppliger, G., Perkins, M., Moeck, I., and Drakos, P., 2010, Structural controls of geothermal activity in the northern Hot Springs Mountains, western Nevada: The tale of three geothermal systems (Brady's, Desert Perk, and Desert Queen): Geothermal Resources Council Transactions, v. 34, p. 675-683.

Faulds, J.E., Hinz, N.H., Coolbaugh, M.F., Ramelli, A.R., Glen, J.M., Ayling, B., Wannamaker, P.E., DeOreo, S., Siler, D.L., and Craig, J.W., 2019, Vectoring into potential blind geothermal systems in Granite Springs Valley, Western Nevada: Application of the play fairway analysis at multiple scales: PROCEEDINGS, 44th Workshop on Geothermal Reservoir Engineering Stanford University, Stanford, California, February 11-13, 2019, SGP-TR-214, 11 p.

Faulds, J.E., Hinz, N.H., Coolbaugh, M.F., Shevenell, L.A., and Siler, D.L., 2016b, Methodologies and strategies for harnessing the vast geothermal potential of Nevada and the

Great Basin region: A summary of recent studies and advances: American Association of Petroleum Geologists, Pacific Section and Rocky Mountain Section Joint Meeting, Las Vegas, Nevada, October 2-5.

Faulds, J.E., Hinz, N.H., Coolbaugh, M.F., Shevenell, L.A., Siler, D.L., dePolo, C.M., Hammond, W.C., Kreemer, C., Oppliger, G., Wannamaker, P.E., Queen, J.H., and Visser, C.F., 2015a, Discovering blind geothermal systems in the Great Basin region: An integrated geologic and geophysical approach for establishing geothermal play fairways: Final report submitted to the Department of Energy (DE- EE0006731), 106 p.

Faulds, J.E., Hinz, N.H., Coolbaugh, M.F., Shevenell, L.A., Siler, D.L., dePolo, C.M., Hammond, W.H., Kreemer, C.W., Oppliger, G., Wannamaker, P.E., Queen, J., and Visser, C., 2015b, Integrated geologic and geophysical approach for establishing geothermal play fairways and discovering blind geothermal systems in the great basin region, western USA: a progress report: Geothermal Resources Council Transactions, v. 39, p. 691-700.

Faulds, J.E., Hinz, N.H., Coolbaugh, M.F., Siler, D.L., Shevenell, L.A., Queen, J.H., dePolo, C.M., Hammond, W.C., and Kreemer, C., 2016c, Discovering geothermal systems in the Great Basin region: an integrated geologic, geochemical, and geophysical approach for establishing geothermal play fairways: Proceedings, 41st Workshop on Geothermal Reservoir Engineering, Stanford University, Stanford, CA, Feb. 22-24, 15 p.

Faulds, J.E., Sadowski, A.J., Coolbaugh, M.F., and Siler, D.L., 2020-this volume, Geothermal play fairway analysis of the Sou Hills, northern Nevada: A major Quaternary accommodation zone in the Great Basin region: Geothermal Resources Council Transactions, Vol. 44, p. X.

Faulds, N.H., and Hinz, N.H., 2015, Favorable tectonic and structural settings of geothermal settings in the Great Basin Region, western USA: Proxies for discovering blind geothermal systems: Proceedings, World Geothermal Congress 2015, Melbourne, Australia, 6 p.

Ferrill, D.A., Winterle, J., Wittmeyer, G., Sims, D., Colton, S., Armstrong, A., Horowitz, A.S., Meyers, W.B., and Simons, F.F., 1999, Stressed rock strains groundwater at Yucca Mountain, Nevada: GSA Today, v. 9, p. 2–9.

Fritz, W.H., 1968, Geologic map and sections of the southern Cherry Creek and northern Egan Ranges, White Pine County, Nevada: Nevada Bureau of Mines and Geology Map 35, scale 1:62,500.

Gwynn, M., Allis, R., Sprinkel, D., Blackett, R., and Hardwick, C., 2014. Geothermal potential in the basins of northeastern Nevada, Geothermal Resources Council Transactions, Vol. 38, p. 1029-1039.

Heidbach, O., Rajabi, M., Cui, X., Fuchs, K., Müller, B., Reinecker, J., Reiter, K., Tingay, M., Wenzel, F., Xie, F. and Ziegler, M.O., 2018. The World Stress Map database release 2016: Crustal stress pattern across scales, Tectonophysics, v. 744, pp. 484-498, https://doi.org/10.1016/j.tecto.2018.07.007

Hinz, N.H., Coolbaugh, M.F., and Faulds, J.E., 2015, Geothermal resource potential assessment – White Pine County, Nevada: Nevada Bureau of Mines and Geology Report 15, 21 p.

Hose, R.K., Blake, M.C., Jr., and Smith, R.M., 1976, Geology and mineral resources of White Pine County: Nevada Bureau of Mines and Geology Bulletin 85, scale 1:250,000, 113 pages.

Kirby, S.M., 2012. “Summary of Compiled Permeability with Depth Measurements for Basin Fill, Igneous, Carbonate, and Siliciclastic Rocks in the Great Basin and Adjoining Regions.” Utah Geological Survey Open-File Report 602, 9 p.

Koehler, R.D., and Wesnousky, S,G., 2011, Late Pleistocene regional extension rate derived from earthquake geology of late Quaternary faults across Great Basin, Nevada between 38.5 and 40 N latitude, Geological Society of America Bulletin, v. 123, no. 3-4, p. 631–650, doi: 10.1130/B30111.1.

McConville, E.G., 2018, Detailed analysis of geothermal potential in Crescent Valley, north-central Nevada [M.S. Thesis]: University of Nevada, Reno, 122 p.

McConville, E.G., Faulds, J.E., Hinz, N.H., Ramelli, A.R., Coolbaugh, M.F., Shevenell, L., Siler, D.L., and Bourdeau-Hernikl, J., 2017, A play fairway approach to geothermal exploration in Crescent Valley, Nevada: Geothermal Resources Council Transactions, v. 41, p. 1213-1221.

Morris, A., Ferrill, D.A., and Henderson, D.B., 1996, Slip-tendency analysis and fault reactivation: Geology, v. 24, p. 275–278.

Siler, D.L., Faulds, J.E., Glen, J.M.G., Hinz, N.H., Witter, J.B., Blake, K., Queen, J., and Fortuna, M., 2019a, Three-dimensional geologic map of the southern Carson Sink, Nevada, including the Fallon FORGE area: U.S. Geological Survey Scientific Investigations Map 3437, pamphlet 22 p., https://doi.org/10.3133/sim3437

Siler, D.L., Faulds, J.E., Hinz, N.H., Dering, G.M., Edwards, J.H., and Mayhew, B.M., 2019b, Three‐dimensional geologic mapping to assess geothermal potential: examples from Nevada and Oregon: Geothermal Energy, v. 7, no. 2, https://doi.org/10.1186/s40517-018-0117-0

Siler, D.L., Faulds, J.E., Mayhew, B., and McNamara, D.D., 2016a, Analysis of the favorability for geothermal fluid flow in 3–D; Astor Pass geothermal prospect, Great Basin, northwestern Nevada, USA: Geothermics, v. 60, p. 1–12, https://doi.org/10.1016/j.geothermics.2015.11.002

Siler, D.L., Hinz, N.H., Faulds, J. E., and Queen, J., 2016b, 3–D analysis of geothermal fluid flow favorability—Brady's, Nevada, USA: Proceedings, Forty-First Workshop on Geothermal Reservoir Engineering, Stanford University, 10 p.

Siler, D.L., Hinz, N.H., Faulds, J.E., 2018. Stress concentrations at structural discontinuities in active fault zones in the western United States: Implications for permeability and fluid flow in geothermal fields. Geological Society of America Bulletin, v. 130. https://doi.org/10.1130/B31729.1

Webring, M.W., 1985. SAKI--A Fortran program for generalized linear inversion of gravity and magnetic profiles: U.S. Geological Survey Open-File Report 85-122, 104 p.